Elastomers and Composites
Vol. 58, No. 4, pp. 191~200 (December 2023)

Print ISSN 2092-9676/Online ISSN 2288-7725
DOI: https://doi.org/10.7473/EC.2023.58.4.191

Optimization of Sonocatalytic Orange II Degradation on MoS_2 Nanoparticles using Response Surface Methodology

Jiulong Li[*], Jeong Won Ko[**], and Weon Bae Ko[*,*,†]**

[*]*Department of Environmental Horticulture, Environmental Chemistry Major, Graduate School, Sahmyook University, 815 Hwarang-ro, Seoul 01795, Republic of Korea*
[**]*Department of Animal Resources Science, Sahmyook University, 815 Hwarang-ro, Seoul 01795, Republic of Korea*
[***]*Department of Chemistry, Sahmyook University, 815 Hwarang-ro, Seoul 01795, Republic of Korea*

(Received December 6, 2023, Revised December 16, 2023, Accepted December 20, 2023)

Abstract: In this study, MoS_2 nanoparticles were synthesized and analyzed through powder X-ray diffraction, Raman, ultraviolet–visible, and X-ray photoelectron spectroscopies. The surface morphologies of the as-synthesized MoS_2 nanoparticles were investigated through scanning and transmission electron microscopies. The sonocatalytic activity of the MoS_2 nanoparticles toward Orange II removal was evaluated by utilizing a Box–Behnken design for response surface methodology in the experimental design. The sonocatalyst dosage, Orange II dye concentration, and ultrasound treatment time were optimized to be 0.49 g/L, 5 mg/L, and 150 min, respectively. The maximum efficiency of Orange II degradation on MoS_2 nanoparticles was achieved, with a final average value of 82.93%. Further, the results of a kinetics study on sonocatalytic Orange II degradation demonstrated that the process fits well with a pseudo-first-order kinetic model.

Keywords: MoS_2 nanoparticles, sonocatalyst, Orange II, Box–Behnken design, response surface methodology

Introduction

In recent years, advanced oxidation processes (AOPs), including Fenton oxidation, photocatalysis, sonocatalysis, and ozonation, have been developed as promising alternative methods for the removal of hazardous pollutants from wastewater.[1-5] Many studies have shown that sonocatalysis is the most attractive treatment for the degradation of organic pollutants compared with other AOPs, owing to its several advantages, such as eco-friendliness, low cost, convenient operation, and high efficiency.[6-8] In the ultrasonic cavitation process, the microbubbles produced by ultrasonic waves provide a high temperature and high pressure environment for the pyrolysis of H_2O molecules via continuous nucleation, growth, and collapse.[9] As a result, •OH radicals having strong oxidation ability are generated, which can subsequently break down a number of organic pollutants into smaller molecules and finally mineralize them into CO_2 and H_2O.[10-12]

MoS_2 has a graphene-like two-dimensional structure which can offer a large specific surface area and excellent adsorption performance.[13,14] Moreover, as a transition metal dichalcogenide (TMD), MoS_2 has attracted tremendous attention and is widely applied in many fields, such as photoelectronics, hydrodeoxygenation (HDO), photocatalysis, and energy devices, owing to its chemical stability, good conductivity, high photosensitivity, and high carrier mobility.[15-17] Over the past few decades, various techniques such as sonolysis, chemical vapor deposition, plasma microwave, and solvothermal or hydrothermal methods have been studied for the preparation of MoS_2 nanoparticles.[18-20] Notably, a decrease in nanocatalyst particle size indicates an increase in surface area, which causes shifts in the valence and conduction band levels.[21] As a result, the indirect band gap energy is increased from a bulk MoS_2 value of ~1.2 eV to a nanoscale MoS_2 value of ~1.8 eV.[22] In our previous work, we investigated the photocatalytic and catalytic behavior of MoS_2 in aqueous media.[23] Although many studies on the application of pure and modified MoS_2 nanomaterials toward the degradation of organic pollutants have been conducted, to the best of our knowledge, the optimization of azo dye degradation via ultrasonic treatment has not been widely conducted.

[†]Corresponding author E-mail: kowb@syu.ac.kr

Hence, this study aimed to investigate the morphology, microstructure, and elemental composition of as-synthesized MoS_2 nanoparticles and to optimize various conditions, namely, sonocatalyst dosage, dye concentration, and ultrasound treatment time for the sonocatalytic degradation process of azo dyes, represented by Orange II. Response surface methodology (RSM) is a statistical method used to determine the optimal conditions in a multi-factor system, which has been widely used in the statistical analysis of wastewater treatment process conditions.[24,25] In this study, RSM experimental design was employed with the Box–Behnken model to obtain the optimum conditions for sonocatalytic degradation of Orange II.

Experimental

1. Materials

Sodium molybdate dihydrate ($Na_2MoO_4 \cdot 2H_2O$) was obtained from Junsei Chemical Co. Ltd. Thioacetamide (TAA, CH_3CSNH_2) was purchased from Tokyo Chemical Industry Co., Ltd. 1-Methyl-2-pyrrolidone (NMP) was obtained from Samchun Chemicals. Hydrochloric acid, ethanol, and Orange II were purchased from Sigma-Aldrich, Inc. All chemical materials with commercial AR purity were used directly without further purification.

2. Synthesis of MoS_2 nanoparticles

In a typical synthesis, 24 mmol of TAA and 4 mmol of sodium molybdate dihydrate were dissolved in an aqueous solution consisting of 100 mL deionized water and 15 mL ethanol. After vigorous stirring for 10 min at room temperature, the mixture was maintained at 90 °C for 5 min. The aqueous solution was then cooled to 80 °C, and 22.5 mL HCl (12 M) was added while stirring. After the addition of HCl, the color of the solution turned dark blue and then quickly turned dark brown. The reaction was maintained at 80 °C for 10 min, and the resultant precipitate was washed several times with deionized water to eliminate additional ions. After drying the precursor at 100 °C for 12 h, it was ground into a powder using a mortar and pestle. Finally, the powder was calcined in an electric furnace (Ajeon Heating Industry Co., Ltd.) at 850 °C for 2 h under an inert argon atmosphere to obtain the MoS_2 nanoparticles.

3. Instruments and characterization methods

Powder X-ray diffraction (XRD, Bruker, D8 ADVANCE) analysis with Cu Kα radiation (λ=1.54178 Å) was performed to identify the structural and crystalline phases of the MoS_2 nanoparticles. The lattice vibrations of the products were characterized via Raman spectroscopy (BWS465 i-Raman Plus) using a laser operating at an excitation wavelength of 532 nm. The chemical states of the MoS_2 nanoparticles were analyzed by X-ray photoelectron spectroscopy (XPS, ESCALAB 250 Xi, Thermo Fisher Scientific) using a monochromatized Al K-alpha X-ray source. The surface morphology was observed using scanning electron microscopy (SEM, Hitachi S-4800). Transmission electron microscopy (TEM) images was conducted using a JEOL JEM-2100 Plus instrument operating at 200 kV.

4. Sonocatalytic performance

For sonocatalytic degradation experiments, ultrasonic treatment was conducted using a Cole-Parmer ultrasonic processor (20 kHz, 500 W). The temperature of the ultrasonic bath was maintained at 25±2 °C using a circulating water bath. For the sonocatalytic reaction, 5-15 mg/L of Orange II were prepared, and the performance of the as-synthesized MoS_2 nanoparticles was evaluated by adding 0.2-0.6 g/L of sonocatalyst to 50 mL of the dye solution via ultrasonic treatment. To achieve an adsorption-desorption equilibrium between the sonocatalyst and Orange II, the mixture was stirred magnetically for 30 min in the dark condition before the ultrasonic treatment.

The Orange II degradation efficiency was determined as follows:

$$\text{Degradation efficiency } (\%) = (1 - C_t/C_0) \times 100\% \quad (1)$$

where C_0 is the initial concentration of Orange II, and C_t is the concentration of dye after reaction time t.

5. Experimental design

To optimize the conditions for the sonocatalytic degradation of Orange II, Box–Behnken design (BBD) was applied with three factors at three levels using Design Expert 12 software. According to the BBD method, 17 runs were performed to evaluate the effects of sonocatalyst dosage, dye

Table 1. Independent Variables and Their Levels for Box-Behnken Design

Independent variables	Units	Symbol	Range and Levels		
			-1	0	1
Sonocatalyst dosage	g/L	X_1	0.2	0.4	0.6
Dye concentration	mg/L	X_2	5	10	15
Ultrasound treatment time	min	X_3	90	120	150

Table 2. Three-factor BBD for RSM with Experimental and Predicted Values of Degradation Efficiency for Orange II at Various Conditions

Run	Factors			Degradation efficiency (%)	
	X_1	X_2	X_3	Experimental	Predicted
1	0	0	0	64.53	66.39
2	1	0	-1	54.14	54.21
3	-1	-1	0	63.10	61.69
4	1	0	1	73.79	73.00
5	-1	1	0	40.58	41.26
6	0	1	-1	42.92	41.44
7	0	0	0	66.85	66.39
8	0	0	0	65.12	66.39
9	-1	0	-1	41.39	42.18
10	0	-1	1	80.35	82.93
11	0	0	0	67.65	66.39
12	-1	0	1	63.36	63.29
13	0	1	1	57.44	56.83
14	1	-1	0	73.25	72.57
15	0	-1	-1	56.7	57.32
16	0	0	0	67.81	66.39
17	1	1	0	50.71	52.12

concentration, and ultrasound treatment time. The levels of different optional variables and RSM designs are listed in Table 1. Response variable (Y) is the degradation efficiency of Orange II and listed in Table 2. The correlation between the response variable and independent variables is expressed by a quadratic polynomial equation, written as follows[26]:

$$Y = \beta_0 + \beta_1X_1 + \beta_2X_2 + \beta_3X_3 + \beta_{12}X_1X_2 + \beta_{13}X_1X_3 + \beta_{23}X_2X_3 + \beta_{11}X_1^2 + \beta_{22}X_2^2 + \beta_{33}X_3^2 \quad (2)$$

where β_0, β_i, β_{ii}, and β_{ij} are the constant coefficient, linear interaction coefficient, quadratic interaction coefficient, and cross-factor interaction coefficients, respectively, and X_1, X_2, and X_3 represent the independent variables as the coded values of sonocatalyst dosage, dye concentration, and ultrasound treatment time, respectively.

Results and Discussion

1. Characterization of the sonocatalyst

XRD was performed to determine the crystalline structure and phase purity of the prepared MoS_2 nanoparticles. As shown in Figure 1, peaks are observed in the XRD pattern at 14.33°, 32.76°, 39.64°, 49.70°, and 58.33° corresponding to the (002), (100), (103), (105), and (110) planes of the hexagonal phase of MoS_2, respectively (JCPDS No. 37-1492).[19] The absence of other peaks indicates that MoS_2 was successfully synthesized with a high purity. The crystallite size of the MoS_2 nanoparticles was calculated using the Scherrer equation:

$$D = \frac{K\lambda}{\beta \cdot \cos\theta} \quad (3)$$

where K is the shape factor considered as 0.9, λ is the wavelength of powder XRD with Cu Kα radiation (λ=1.54178 Å), β is the full width at half maximum (FWHM, β=0.51˚), and 2θ is the angle between the incident and scattered X-rays. Using this formula, the crystallite size of as-synthesized MoS_2 nanoparticles at (002) plane was determined to be 15.71 nm.

Figure 2 shows the Raman spectra of the MoS_2 nanoparticles. Two distinct Raman peaks are observed at 376 and 402 cm^{-1} corresponding to the in-plane E^1_{2g} and out-of-plane A_{1g} vibrational modes, respectively.[27] The presence of the E^1_{2g} and A_{1g} vibrational modes implies that the samples have a 2H-MoS_2 structure. In addition, a 36 cm^{-1} discrepancy in the Raman shift between the E^1_{2g} and A_{1g} vibrational modes indi-

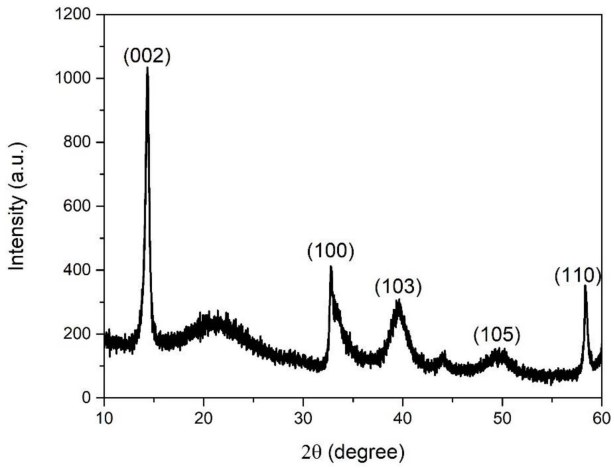

Figure 1. XRD patterns of the as-synthesized MoS_2 nanoparticles.

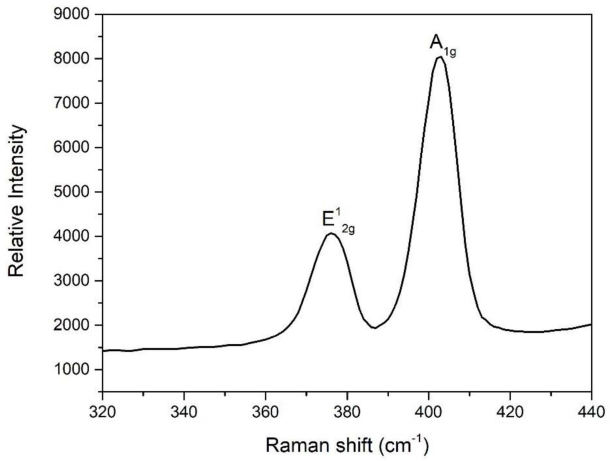

Figure 2. Raman spectra of the as-synthesized MoS_2 nanoparticles.

cated that as-synthesized MoS_2 had good crystallinity and was multilayered.[28]

UV-vis absorption spectroscopy was performed to investigate the optical properties of the as-synthesized MoS_2 nanoparticles. To obtain a well-dispersed solution, MoS_2 powder was dispersed in the organic solvent of N-methylpyrrolidone (NMP) via ultrasonic treatment for 2 h. The

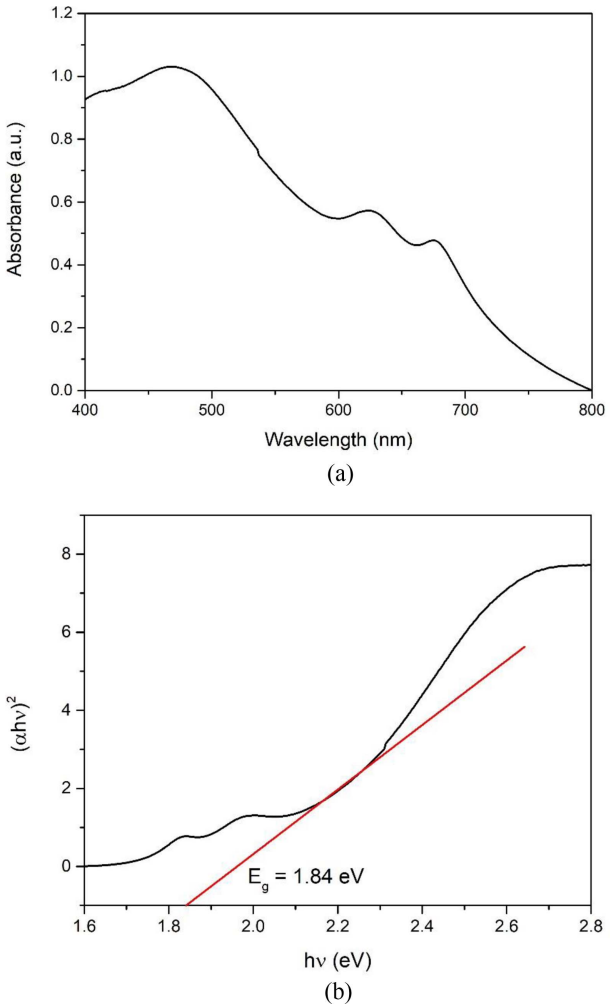

Figure 3. (a) UV-vis absorbance spectra and (b) UV-vis diffuse reflectance spectra of the MoS_2 nanoparticles in NMP.

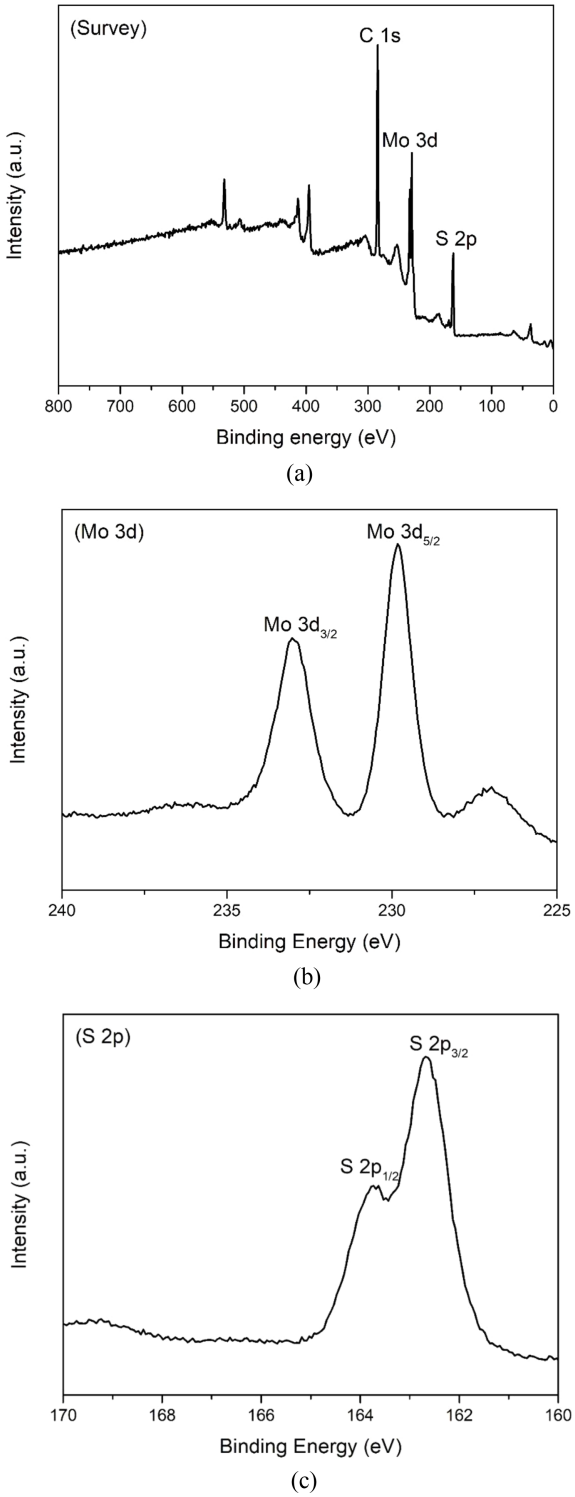

Figure 4. XPS spectra of the MoS_2 nanoparticles (a) full spectra, (b) Mo 3d, (c) S 2p.

UV-vis spectra of the MoS_2 nanoparticles are shown in Figure 3(a). The absorption peaks were observed at 469, 624, and 675 nm. The peak at 469 nm is attributed to a threshold transition between the valence and conduction bands.[29] The band-gap energy of the MoS_2 nanoparticles was determined using the Tauc equation[30]:

$$(\alpha h\nu)^2 = B(h\nu - E_g) \quad (4)$$

where α, h, and ν are the absorption coefficient, Plank's constant, and the light frequency, respectively. B is a constant and E_g is the band-gap energy. As shown in Figure 3(b), the band-gap energy of the as-synthesized MoS_2 nanoparticles was 1.84 eV.

The electronic states of the samples were identified using XPS analysis. The survey spectrum of the MoS_2 nanoparticles in Figure 4(a) shows three major peaks corresponding to Mo 3d, S 2p, and C 1s. The C 1s peak observed at 284.81 eV can be attributed to the hydrocarbons in the XPS system and a small amount of carbon residue on the surface of the samples generated during the synthesis process.[31] The Mo 3d spectrum in Figure 4(b) shows two strong peaks with binding energy values of 229.83 and 233.03 eV corresponding to Mo $3d_{5/2}$ and Mo $3d_{3/2}$, respectively, revealing the presence of Mo^{4+} in the samples.[32] In Figure 4(c), the S 2p spectrum can be deconvoluted into two peaks located at 162.68 and 163.73 eV, which are attributed to the S $2p_{3/2}$ and S $2p_{1/2}$ of the S^{2-} state in the MoS_2 nanoparticles, respectively.[33]

The morphological and structural information of the products was determined using SEM and TEM images. As can be seen in Figure 5, the synthesized MoS_2 nanoparticles were connected to each other by the aggregation of irregular-shaped grains. The size of MoS_2 is between 50 and 100 nm.

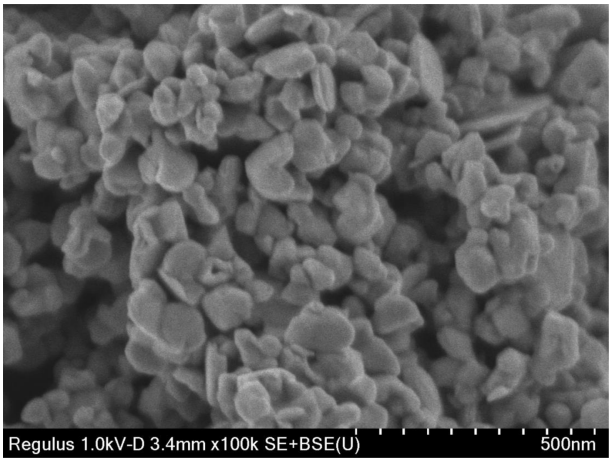

Figure 5. SEM image of the MoS_2 nanoparticles.

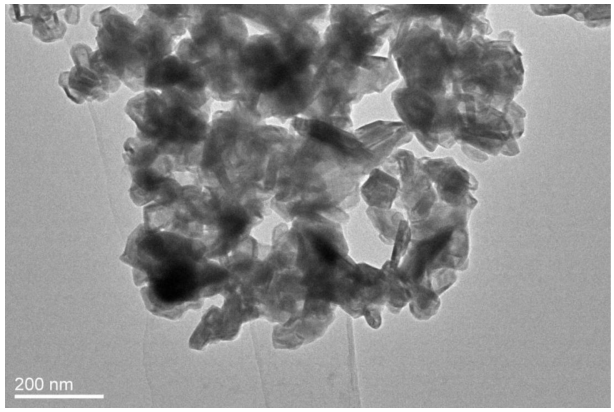

Figure 6. TEM image of the MoS_2 nanoparticles.

In Figure 6, the TEM image of synthesized MoS_2 nanoparticles was shown to have a rag structure, and several MoS_2 layers were disorderly folded in the rag structure.

2. BBD model validation and statistical analysis

The sonocatalytic Orange II degradation experiments were performed using the BBD. The experimental results are summarized in Table 2; the Orange II degradation efficiency ranged from 40.58 to 80.35%. Based on the results in Table 2, the quadratic polynomial regression equation showing the dependence of the Orange II degradation efficiency on the three independent variables, namely, sonocatalyst dosage, dye concentration, and ultrasound treatment time, can be expressed as follows:

$$Y = 66.39 + 5.43X_1 - 10.22X_2 + 9.97X_3 - 0.005X_1X_2 - 0.58X_1X_3 - 2.28X_2X_3 - 5.33X_1^2 - 4.15X_2^2 - 2.89X_3^2 \quad (5)$$

To verify the fit of the model, analysis of variance (ANOVA) for the three independent variables was conducted on the basis of the experimental data. The ANOVA results for dye degradation are summarized in Table 3. For this study, high F-value (82.52 and low p-value (<0.0001) indicated that the model was significant. The p-values of the main variables were <0.0001, demonstrating the statistical significance of each variable for the sonocatalytic Orange II degradation. An analysis for lack of fit gives an F-value of 1.69 and a p-value of 0.3048 (>0.05), showing that lack of fit is insignificant.[34] Therefore, the quadratic regression model fits well with the obtained data and effectively predicts the experimental results. The determination coefficient (R^2), adjusted determination coefficient (R_{adj}^2), and predicted

Table 3. ANOVA Analysis of the BBD Quadratic Modeling in the Optimization of the Sonocatalytic Activity of MoS_2 for the Degradation of Orange II

Source	Sum of Squares	df	Mean Square	F-value	p-value
Model	2141.5	9	237.94	82.52	<0.0001
X_1	236.1	1	236.1	81.88	<0.0001
X_2	835.38	1	835.38	289.71	<0.0001
X_3	795.81	1	795.81	275.99	<0.0001
X_1X_2	0.0001	1	0.0001	0	0.9955
X_1X_3	1.35	1	1.35	0.4667	0.5165
X_2X_3	20.84	1	20.84	7.23	0.0312
X_1^2	119.72	1	119.72	41.52	0.0004
X_2^2	72.51	1	72.51	25.15	0.0015
X_3^2	35.16	1	35.16	12.19	0.0101
Residual	20.18	7	2.88	–	–
Lack of Fit	11.3	3	3.77	1.69	0.3048
Pure Error	8.89	4	2.22	–	–
Cor Total	2161.68	6	–	–	–

$R^2 = 0.9907$, $R_{adj}^2 = 0.9787$, $R_{pred}^2 = 0.9100$

determination coefficient (R_{pred}^2) for the regression equation are 0.9907, 0.9787, and 0.9100, respectively. The R^2 and R_{adj}^2 values were close to 1, indicating a strong correlation between the experimental and predicted values. The difference of R_{adj}^2 and R_{pred}^2 is less than 0.2, indicating that R_{pred}^2 is in reasonable agreement with R_{adj}^2.[26] Based on the results in Figure 7, the experimental and predicted values showed good agreement between the experimental results, and the responses were well predicted by the second-order polynomial model.

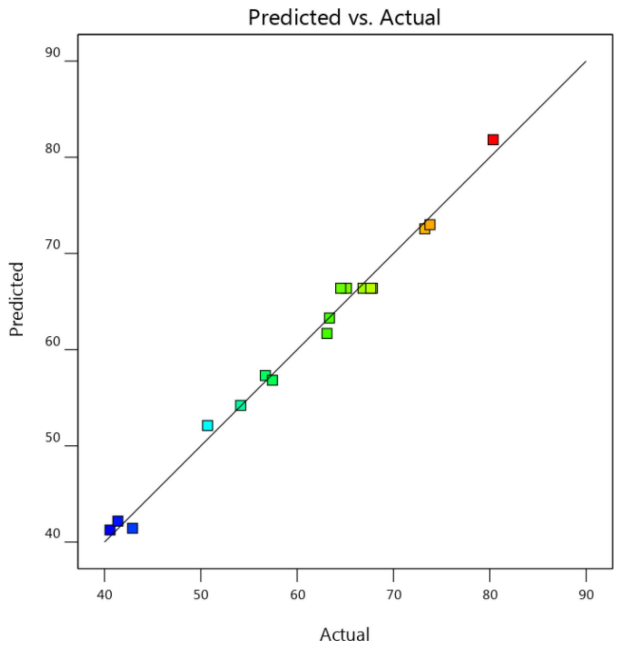

Figure 7. Graphical plot of predicted vs. actual values for sonocatalytic Orange II degradation on MoS_2 nanoparticles.

3. Effect of independent variables on the sonocatalytic Orange II degradation

A second-order polynomial equation reveal the type of interaction between two variables by fixing a single variable. This interaction can be reflected more visually by three-dimensional response surface plots and contour plots, which show the significance of the interaction between the two variables.

Figure 8(a) and (b) show the interaction between the initial Orange II concentration and sonocatalyst dosage at a constant ultrasound treatment time. The dye degradation efficiency was improved to some extent by increasing the sonocatalyst dosage. However, the dye degradation efficiency decreased rapidly with an increase in the initial Orange II concentration. This is because at a high initial dye concentration, more dye molecules are adsorbed onto the surface of the sonocatalyst, which leads to a substantial weakening of the effect of sonocatalysis. The lowest degradation efficiency of 40.58% was obtained at a dye concentration of 15 mg/L and a sonocatalyst dosage of 0.2 g/L.

Figure 8(c) and (d) represent the effect of the sonocatalyst dosage and ultrasound treatment time on the dye degradation efficiency at an initial dye concentration of 10 mg/L. It can be clearly seen that an increase in the ultrasound treatment

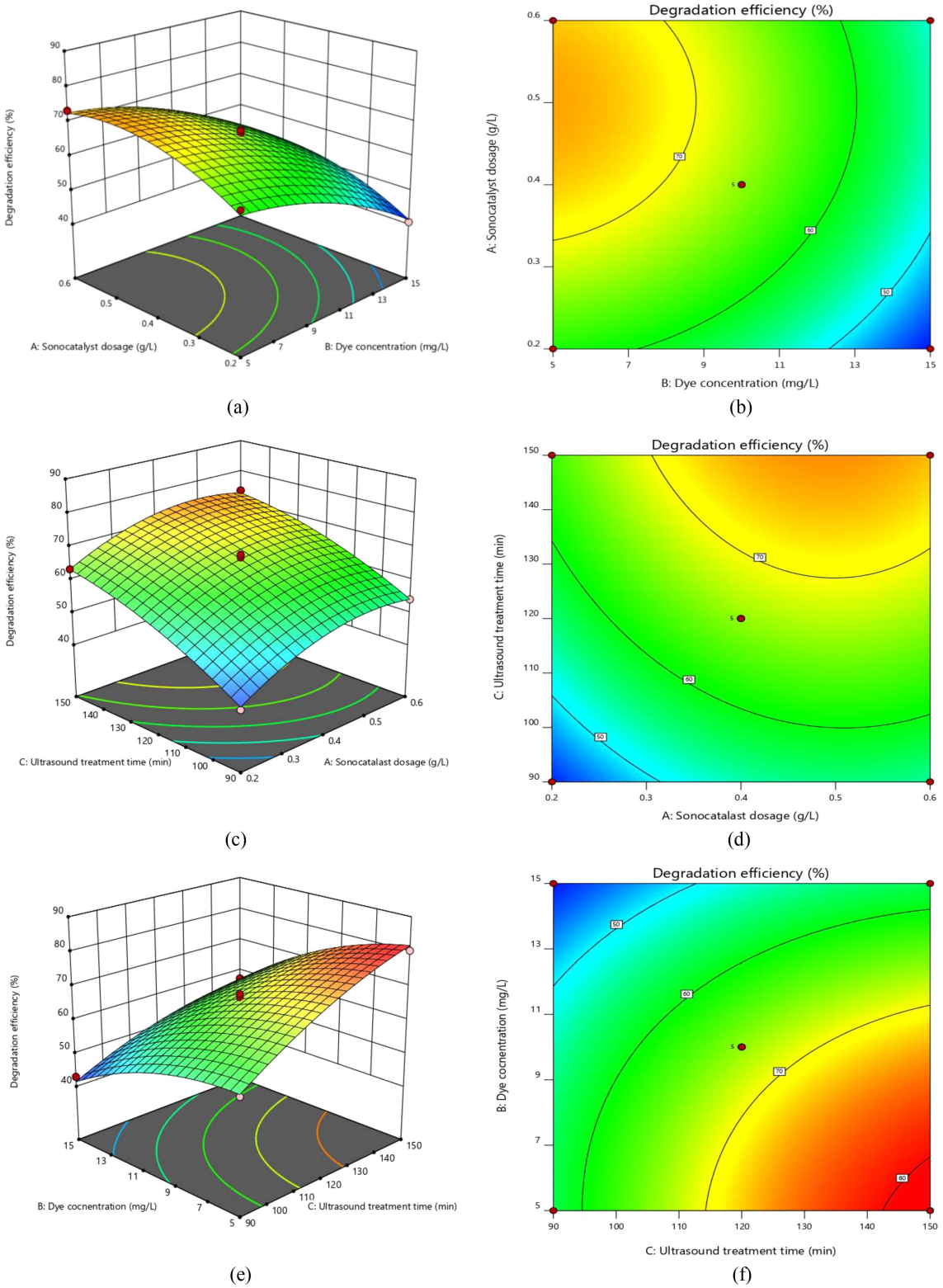

Figure 8. 3D response surface and contour plots for the sonocatalytic Orange II degradation: effects of (a,b) dye concentration and sonocatalyst dosage; (c,d) sonocatalyst dosage and ultrasound treatment time; and (e,f) ultrasound treatment time and dye concentration.

time plays a crucial role in improving the Orange II degradation efficiency. In addition, we found that the magnitude of the change in degradation efficiency caused by an increase in sonocatalyst dosage from 0.4 to 0.6 g/L was lower than

that caused by an increase from 0.2 to 0.4 g/L. This may be due to the addition of excessive sonocatalyst, which reduces the dispersion in the system and adversely affects the availability of surface active sites due to local aggregation of the sonocatalyst.

Figure 8(e) and (f) show the effects of the ultrasound treatment time and initial Orange II concentration on the dye degradation efficiency for a fixed dosage of sonocatalyst. With increasing ultrasound treatment time, the degree of ultrasonic cavitation is enhanced, which resulted in the involvement of more reactive radicals in the oxidation of the dye. In this set of experiments, the highest dye degradation efficiency was obtained at an ultrasound treatment time of 150 min, an initial dye concentration of 5 mg/L, and a sonocatalyst dosage of 0.4 g/L. The maximum Orange II degradation efficiency was 80.35%.

4. Optimum condition and verification of the model

Optimizing the numerical values and determining the operational parameters to achieve maximum degradation efficiency were the primary goals of the experimental design. In this study, the experimental conditions were limited to a sonocatalyst dosage of 0.2-0.6 g/L, an Orange II concentration of 5 to 15 mg/L, and ultrasound treatment time of 90-150 min. The operational parameters were optimized to be sonocatalyst dosage of 0.49 g/L, an Orange II dye concentration of 5 mg/L, and an ultrasound treatment time of 150 min by using the optimization function in Design Expert 12. The optimal dye degradation efficiency was predicted to be 82.93% (Figure 9). The error between the model prediction and experimental values was found to be ~3%, demonstrating the accuracy and reliability of the model optimization applied in the sonocatalytic Orange II degradation experiments.

5. Kinetics study of sonocatalytic degradation

Based on the above experimental results under the optimized conditions, the kinetics of the Orange II degradation on the as-synthesized MoS_2 serving as a sonocatalyst was investigated using the Langmuir–Hinshelwood model, which has been widely applied as a model for pseudo-first-order kinetic processes.[29,35]

The kinetic equation is as follows:

$$\ln (C_t/C_0) = -kt \quad (6)$$

where C_0 is the Orange II concentration after adsorption, C_t is the dye concentration at reaction time t, and k is the rate

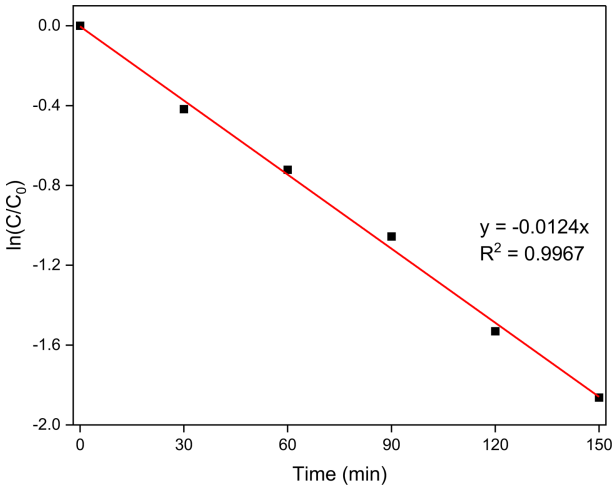

Figure 10. Results of kinetics study on Orange II degradation under the optimized conditions.

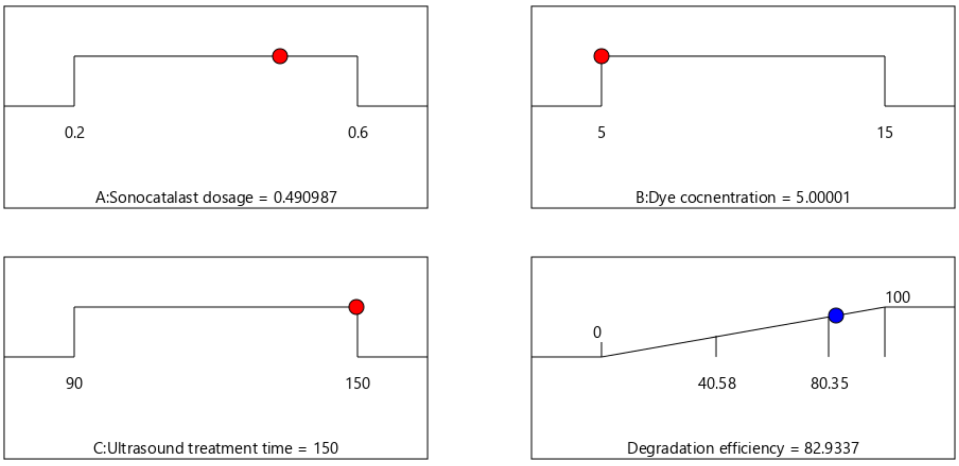

Figure 9. Scheme of optimum operational parameters for sonocatalytic Orange II degradation on MoS_2 nanoparticles.

constant of sonocatalytic degradation. Figure 10 shows a plot of ln (C_t/C_0) versus the ultrasonic treatment time under the optimized conditions. The rate constant was determined to be 0.0124 min^{-1}. Moreover, the square of the linear correlation coefficient (R^2) was >0.99, indicating that the sonocatalytic Orange II degradation on the MoS_2 nanoparticles fit well with the pseudo-first-order model.

Conclusions

MoS_2 nanoparticles were successfully synthesized using a simple hydrothermal and calcination method. XRD, Raman spectroscopy, UV-vis spectroscopy, XPS, SEM, and TEM were used to characterize the as-synthesized MoS_2 nanoparticles. The sonocatalytic activity of the samples toward Orange II degradation were evaluated.

The RSM based on BBD approach was utilized to explore the effects of the operational parameters on Orange II dye removal.

The ANOVA results demonstrated that the regression model is highly reliable in predicting the Orange II degradation efficiency. The optimal degradation efficiency (82.93 %) was achieved at a sonocatalyst dosage of 0.49 g/L, an orange II dye concentration of 5 mg/L, and an ultrasound treatment time of 150 min. Moreover, the results of the kinetics study indicated that the sonocatalytic Orange II degradation on the MoS_2 nanoparticles fit well with the pseudo-first-order model.

Acknowledgements

This study was supported by research funding from Sahmyook University in Korea.

Conflict of Interest: The authors declare that there is no conflict of interest.

References

1. N. A. Jamalluddin and A. Z. Abdullah, "Reactive dye degradation by combined Fe (III)/TiO_2 catalyst and ultrasonic irradiation: Effect of Fe (III) loading and calcination temperature", *Ultrason. Sonochem.*, **18**, 669 (2011).
2. A. Hassani, A. Khataee, S. Karaca, C. Karaca, and P. Gholami, "Sonocatalytic degradation of ciproflfloxacin using synthesized TiO_2 nanoparticles on montmorillonite", *Ultrason. Sonochem.*, **35**, 251 (2017).
3. M. Dukkanci, "Sono-photo-Fenton oxidation of bisphenol-A over a $LaFeO_3$ perovskite catalyst", *Ultrason. Sonochem.*, **40**, 110 (2018).
4. E. K. Lee and S. Y. Han, "Synthesis and Characterization of the Ag-doped TiO_2", *Elast. Compos.*, **57**, 1 (2022).
5. J. Li, J. W. Ko, and W. B. Ko, "Photocatalytic Degradation of Organic Dyes using CdSe-Mn-C_{60} Nanocomposites", *Elast. Compos*., **57**, 181 (2022).
6. Y. Panahian and N. Arsalani, "Synthesis of hedgehog-like F-TiO_2(B)/CNT nanocomposites for sonophotocatalytic and photocatalytic degradation of malachite green (MG) under visible light: kinetic study", *J. Phys. Chem.*, **121**, 5614 (2017).
7. A. Maroudas, P. K. Pandis, A. Chatzopoulou, L. R. Davellas, G. Sourkouni, and C. Argirusis, "Synergetic decolorization of azo dyes using ultrasounds, photocatalysis and photo-fenton reaction", *Ultrason. Sonochem.*, **71**, 105367 (2021).
8. A. Khataee, P. Eghbali, M. H. Irani-Nezhad, and A. Hassani, "Sonochemical synthesis of WS_2 nanosheets and its application in sonocatalytic removal of organic dyes from water solution", *Ultrason. Sonochem.*, **48**, 329 (2018).
9. N. Ertugay and F. N. Acar, "The degradation of direct blue 71 by sono, photo and sonophotocatalytic oxidation in the presence of ZnO nanocatalyst", *Appl. Surf. Sci.*, **318**, 121 (2014).
10. R. J. Ramalingam, G. Periyasami, M. Ouladsmane, Z. A. Alothman, P. Arunachalam, T. Altalhi, T. Radhika, and A. G. Alanazi, "Ultra-sonication assisted metal chalcogenide modified mesoporous Nickel-cobalt doped manganese oxide nanocomposite fabrication for sono-catalytic dye degradation and mechanism insights", *J. Alloys Compd.*, **875**, 160072 (2021).
11. P. Qiu, B. Park, J. Choi, B. Thokchom, A. B. Pandit, and J. Khim, "A review on heterogeneous sonocatalyst for treatment of organic pollutants in aqueous phase based on catalytic mechanism", *Ultrason. Sonochem.*, **45**, 29 (2018).
12. R. Balachandran, Z. Patterson, P. Deymier, S. A. Snyder, and M. Keswani, "Understanding acoustic cavitation for sonolytic degradation of p-cresol as a model contaminant", *Chemosphere*, **147**, 52 (2016).
13. S. V. P. Vattikuti, S. Shome, G. Koyyada, J. Shim, and J. H. Jung, "Fabrication of highly efficient carbon coated exfoliated tungsten disulfide nanosheets core-shell nanostructure as a promising solar-light driven photocatalyst", *Mater. Res. Bull.*, **107**, 446 (2018).
14. H. J. Song, S. You, X. H. Jia, and J. Yang, "MoS_2 nanosheets decorated with magnetic Fe_3O_4 nanoparticles and their ultrafast adsorption for wastewater treatment", *Ceram. Int.*, **41**, 13896 (2015).

15. M. A. Hossain, B. A. Merzougui, F. H. Alharbi, and N. Tabet, "Electrochemical deposition of bulk MoS_2 thin films for photovoltaic applications", *Sol. Energy Mater. Sol. Cells*, **186**, 165 (2018).
16. W. Wang, L. Li, S. Tan, K. Wu, G. Zhu, Y. Liu, Y. Xu, and Y. Yang, "Preparation of NiS_2//MoS_2 catalysts by two-step hydrothermal method and their enhanced activity for hydrodeoxygenation of p-cresol", *Fuel*, **179**, 1 (2016).
17. C. N. R. Rao, U. Maitra, and U. V. Waghmare, "Extraordinary attributes of 2-dimensional MoS_2 nanosheets", *Chem. Phys. Lett.*, **609**, 172 (2014).
18. B. Pourabbas and B. Jamshidi, "Preparation of MoS_2 nanoparticles by a modified hydrothermal method and the photo-catalytic activity of MoS_2/TiO_2 hybrids in photo-oxidation of phenol", *Chem. Eng. J.*, **138**, 55 (2008).
19. Y. Xu, E. Z. Hu, and H. Hu, "Formation of an adsorption film of MoS_2 nanoparticles and dioctyl sebacate on a steel surface for alleviating friction and wear", *Tribol. Int.*, **92**, 172 (2015).
20. H. Liu, T. Lv, C. K. Zhu, X. Su, and Z. Zhu, "Efficient synthesis of MoS_2 nanoparticles modified TiO_2 nanobelts with enhanced visible-light-driven photocatalytic activity", *J. Mol. Catal. A: Chem.*, **396**, 136 (2015).
21. S. A. Darsara, M. Seifi, and M. B. Askari, "One-step hydrothermal synthesisi of MoS_2/CdS nanocomposite and study of structural, photocatalytic, and optical properties of this nanocomposite", *Optik*, **169**, 249 (2018).
22. D. James and T. Zubkov, "Photocatalytic properties of free and oxide-supported MoS_2 and WS_2 nanoparticles synthesized without surfactants", *J. Photochem. Photobio. A: Chem.*, **262**, 45 (2013).
23. J. L. Li and W. B. Ko, "Facile synthesis of MoS_2-C_{60} nanocomposites and their application to catalytic reduction and photocatalytic degradation", *Elastomers and Composites*, **51**, 286 (2016).
24. G. Swain, S. Singh, R. K. Sonwani, R. S. Singh, R. P. Jaiswal, and B. N. Rai, "Removal of acid orange 7 dye in a packed bed bioreactor: Process optimization using response surface methodology and kinetic study", *Bioresou. Technol.*, **13**, 100620 (2021).
25. S. G. Jeon, J. W. Ko, and W. B. Ko, "Ultrasound assisted synthesis of gadolinium oxide-zeolitic imidazolate framework-8 nanocomposites and their optimization for photocatalytic degradation of methyl orange using response surface methodology", *Catalysts*, **11**, 1022 (2021).
26. R. Mahdavi and S. S. A. Talesh, "Enhancement of ultrasound-assisted degradation of Eosin B in the presence of nanoparticles of ZnO as sonocatalyst", *Ultrason. Sonochem.*, **51**, 230 (2019).
27. L. Q. Su, Y. Zhang, Y. F. Yu, and L. Cao, "Dependence of coupling of quasi 2-D MoS_2 with substrates on substrate types, probed by temperature dependent Raman scattering", *Nanoscale*, **6**, 4920 (2014).
28. R. Xie, Y. Li, H. Huang, H. Hu, T. Li, B. Guo, L. Su, X. Zhang, G. Xu, L. Wang, F. Chi, H. Liu, and Y. Ma, "Fabrication, structural and vibrational properties, and physical and optical properties tailoring of nanocrystalline MoS_2 films", *Ceram. Int.*, **45**, 18501 (2019).
29. A. K. Mishra, K. V. Lakshmi, and L. Huang, "Eco-friendly synthesis of metal dichalcogenides nanosheets and their environmental remediation potential driven by visible light", *Sci. Rep.*, **5**, 15718 (2015).
30. P. S. Selvamani, J. J. Vijaya, L. J. Kennedy, A. Mustafa, M. Bououdina, P. J. Sophia, and R. J. Ramalingam, "Synergic effect of Cu_2O/MoS_2/rGO for the sonophotocatalytic degradation of tetracycline and ciprofloxacin antibiotics", *Ceram. Int.*, **47**, 4226 (2021).
31. M. O. Ansari, R. Kumar, A. Alshahrie, M. S. Abdel-wahab, V. K. Sajith, M. S. Ansari, A. Jilani, M. A. Barakat, and R. Darwesh, "CuO sputtered flexible polyaniline@graphene thin films: A recyclable photocatalyst with enhanced electrical properties", *Compos. B Eng.*, **175**, 107092 (2019).
32. F. Zhang, W. Zhang, W. Zhu, B. Cheng, H. Qiu, and S. Qi, "Core-shell nanostructured CS/MoS_2: a promising material for microwave absorption", *Appl. Surf. Sci.*, **463**, 182 (2019).
33. I. M. Alarifi, Y. O. Al-Ghamdi, R. Darwesh, M. O. Ansari, and M. K. Uddin, "Properties and application of MoS_2 nanopowder: characterization, congo red dye adsorption, and optimization", *J. Mater. Res. Technol.*, **13**, 1169 (2021).
34. H. Chaker, A. E. Attar, M. Djennas, and S. Fourmentin, "A statistical modeling-optimization approach for effifficiency photocatalytic degradation of textile azo dye using cerium-doped mesoporous ZnO: A central composite design in response surface methodology", *Chem. Eng. Res. Des.*, **171**, 198 (2021).
35. L. M. Song, S. J. Zhang, X. Q. Wu, and Q. Wei, "Synthesis of porous and trigonal TiO_2 nanoflake, its high activity for sonocatalytic degradation of rhodamine B and kinetic analysis", *Ultrason. Sonochem.*, **19**, 1169 (2012).